Available online at www.sciencedirect.com
SCIENCE DIRECT®
Solid State Ionics 165 (2003) 43–49
SOLID STATE IONICS
www.elsevier.com/locate/ssi

Oxygen vacancy in cubic WO_3 studied by first-principles pseudopotential calculation

S.Zh. Karazhanov[a], Yong Zhang[a,*], A. Mascarenhas[a], S. Deb[a], L.-W. Wang[b]

[a] National Renewable Energy Laboratory, 1617 Cole Boulevard, Golden, CO 80401, USA
[b] NERSC, Lawrence Berkeley National Laboratory, Berkeley, CA 94720, USA

Abstract

In this work, the oxygen vacancy in WO_3 has been studied by an ab initio pseudopotential method within the local density approximation (LDA). It is shown that with the charge state change of the vacancy, a strong lattice relaxation, swing from one to the other side of the un-relaxed position, is found for the nearest W ions, accompanied by large changes in the electronic structure of the vacancy. It is found that an oxygen vacancy in WO_3 gives rise to three types of defect states: a donor-like state near the fundamental band gap, derived from the top valence bands, a hyper-deep resonant state in the valence band and a high-lying resonant state in the conduction band, derived from the oxygen 2s bonding and anti-bonding band, respectively. The existence of the donor-like defect state offers a possible explanation for the dependence of the conductivity and the mid-gap absorption on the O deficiency.

PACS: 31.15.Ar; 61.72.Ji; 71.00.00; 71.15.Ap; 71.15.Fv; 71.15.Mb; 71.20−b; 77.84.Dy; 78.20.Jq; 74.25.Jb
Keywords: ABO_3 perovskites; Tungsten oxide; Electrochromism; Non-stoichiometry; Defects; Ab initio calculations; LDA; Pseudopotential methods

Tungsten oxide is one of the most intensively studied electrochromic materials because of its many technologically important electro-optic, electrochromic, ferroelectric, and semiconducting properties [1–3]. Despite the three decades of intense studies, the physical mechanism for the coloration still remains controversial [1,4–6] and the origin of the mid-gap optical transition is not clear. Deb's vacancy model [1] suggests that the oxygen vacancy (V_O) is involved in the optical transition; while all the other models suggest that the optical transition occurs via the charge transfer between non-equivalent W sites in one way or the other [4–6]. It is found in Ref. [7] that the electrochromic colouration efficiency and conductivity is enhanced, and the peak energy of the mid-gap absorption shifts to the higher energy, with increasing oxygen deficiency.

There have been numerous theoretical studies on the electronic structure of WO_3 with and without ion intercalation: non-self-consistent and/or semi-empirical calculations [8–11], and self-consistent first-principles calculations [12–16]. However, no publications on the theoretical study of V_O in WO_3 system either with or without the intercalation have been found except for one for amorphous WO_3 [17]. Nevertheless, the properties of V_O in a related system, $KNbO_3$, have indeed been studied [18,19]. Here, we perform a

* Corresponding author.
E-mail address: yong_zhang@nrel.gov (Y. Zhang).

0167-2738/$ - see front matter © 2003 Elsevier B.V. All rights reserved.
doi:10.1016/j.ssi.2003.08.012

theoretical investigation for the structural and electronic properties of V_O in a cubic WO_3. Although in the real world WO_3 often appears in different structures with lower symmetry than cubic, we believe that this simple structure is a logic starting point along the line of approaching reality.

This investigation was carried out by an ab-initio pseudopotential method within the local density approximation (LDA). Spin-orbit coupling was neglected. Norm-conserving pseudopotentials have been generated using the conjugate gradient algorithm. Pulay–Kerker scheme has been used for self-consistent potential mixing. Also, real space Kleinman–Bylander non-local pseudopotential implementations have been used with a mask function scheme, without the need for preprocessing for the pseudopotentials. We have considered 5d, 6s and 6p as valence states to build the pseudopotential, and 2s, 2p as valence states for the *O* pseudopotential. The energy cutoff for the plane wave basis was 70 Ry. "k-projection" and "band-projection" is performed for identifying the character of any state of interest.

The primitive unit cell with volume Ω_0, for the cubic WO_3 contains four atoms: three O atoms at (0,0,0), (0,*a*/2,*a*/2), and (*a*/2,0,*a*/2) and one W at (0,0,*a*/2) (Fig. 1), where *a* is the lattice constant. The defect structure is simulated by a supercell of size $n_1 \times n_2 \times n_3\ \Omega_0$ with the O atom at the origin removed. Here n_1, n_2 and n_3 are the number of the primitive unit cells along [100], [010] and [001] directions, respectively. The defect structure has a local symmetry of C_{4v} [18], with the symmetry axis along [001]. Three supercell sizes, with 32, 48 and 64 atomic sites (Fig. 1), respectively, have been used to mimic the interaction of the vacancies, by choosing $n_3 = 2$, 3, and 4 and $n_1 = n_2 = 2$. All atomic configurations are obtained by minimizing total energy. For the three supercell structures, we used these special k points in $2\pi/a$: (1/4, 1/4,1/4), (1/4,1/4,1/2) and (1/4,1/4,1/2), respectively, for the self-consistent calculations. The band structure calculation is performed using the charge distribution obtained in the self-consistent calculation.

To test the reliability of the method and establish the reference, we have first performed a detailed calculation for the ideal WO_3. The results of $a = 3.84$ Å and $E_g = 0.43$ eV agree quite well with those of previous self-consistent calculations: $a = 3.73–3.84$ Å and $E_g = 0.3–0.6$ eV [12–16], as well as the experimental

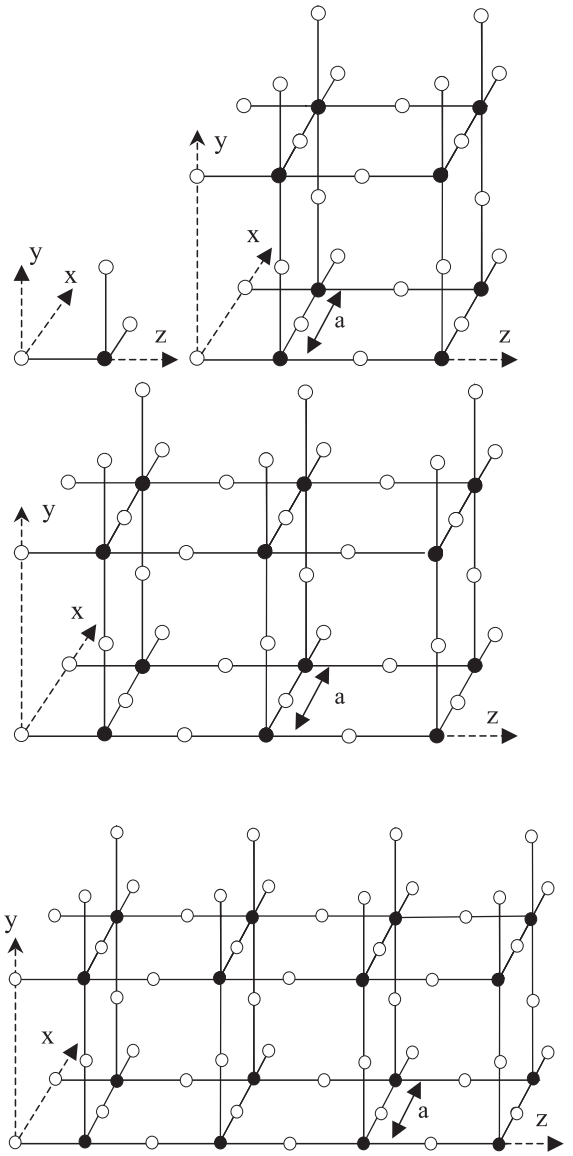

Fig. 1. Schematic presentation of the primitive four-atom unit cell and 32-, 48- and 64-atom supercells.

value of $a = 3.71–3.75$ Å [20]. The band gap, however, is much smaller than the experimental value of 2.62 eV (for monoclinic phase) [21] due to the well-known LDA error. Fig. 2 shows the dispersion curves, which are in general agreement with those of previous calculations [12–16].

The maximum of the valence band is situated at the R point in the Brillioin zone and the minimum of the

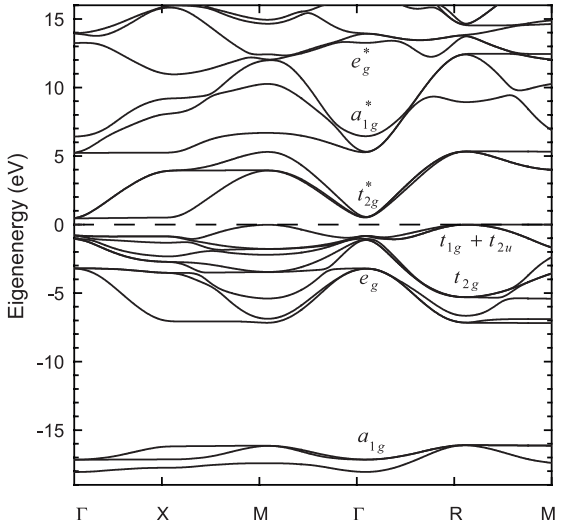

Fig. 2. Electronic band structure of the four-atom primitive cell of cubic WO_3 along several high symmetry lines in the Brillouin zone. The energy reference is at the top of the valence band (R-point), and the Γ conduction band minimum is at 0.43 eV.

conduction band is at the Γ-point. The width of the valence band is 7.29 eV and the direct band gap is 1.2265 eV. The valence band is composed of 12 levels, which can be divided into four bands: three bonding and one non-bonding bands of hybridized *O* 2s, 2p, and *W* 5d and 6s states. A charge distribution analysis shows that the lowest three states form the a_{1g} band, which mainly originates from the O 2s orbitals slightly hybridizing with W 5d(x^2-y^2) and 5d(z^2) states. The next three states form the e_g band, which is due to hybridization of *W* 5d(z^2) and 5d(x^2-y^2) orbitals with *O* 2p orbitals. This band is lower in energy than the t_{2g} band, because the overlapping of the d orbitals for this band with *O* 2p orbitals is stronger than that for the t_{2g} band arising from the interaction between *W* 5 (d_{xy}, d_{xz}, d_{yz}) and *O* 2p orbitals. Respectively, in the conduction band the t_{2g} antibonding band is lower in energy than the e_g^* anti-bonding band. Note that between these two bands it is the a_{1g}^* anti-bonding band. The rest three levels at the top of valence band form $t_{1g}+t_{2u}$ non-bonding band due to nearest *O*–*O* interactions.

For a given supercell structure of the ideal cubic WO_3, the number of occupied valence states equals to $N_0=24$ ($n_1\times n_2\times n_3$)/2, the factor 2 is due to the spin degeneracy. With the removal of one O, the number of occupied states is expected to be $N=N_0-3$. We find that for all the three supercell defect structures, there are only N_0-4 states remaining in the valence band (VB). More specifically, one state is removed from the lowest VB, the "a_{1g}" band. The other three states are removed from the highest VB, the $t_{1g}+t_{2u}$. Note that now the valence band has one state short to accommodate all the valence electrons. Thus, which excited state should the two "extra" electrons occupy is an interesting issue.

After the oxygen atom has been removed, the supercells have been relaxed and optimal atomic positions have been found via a search of the total energy minimum for the double positively charged vacancy V_O^{++} and neutral V_O^o. Fig. 3 presents displacement of the atoms near the vacancy, which exhibits the largest shift from the equilibrium position. We find that for V_O^{++}, the nearest two W ions move outward from their ideal

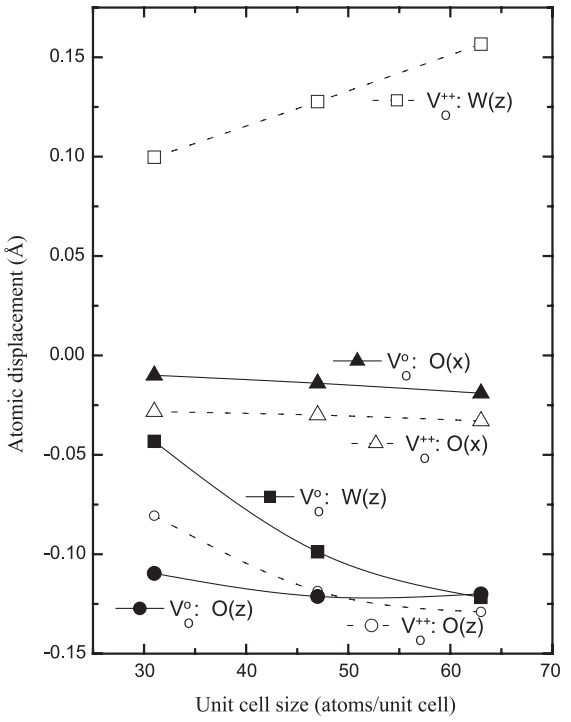

Fig. 3. The dependences of atomic relaxation, along the *z* and *x* directions, for the O and W ions nearest to the vacancy on the supercell size and the vacancy charging state.

positions, due to the loss of the Coulomb attraction from the O ion used to be at the origin; while the eight nearest O ions move towards the vacancy, due to the loss of the balancing repulsion from the O ion. For V_O^o, we find that the nearest W ions now move towards the vacancy, due to the attraction of the two added electrons at the "vacancy site"; and those nearest O ions move back slightly, due to the restored repulsion. Note that the largest displacements have been shown along the [001] direction, while those along other directions [010] and [100] are much smaller.

Analysis of Fig. 3 shows that the displacements depend on not only the charge state of the vacancy, but also the supercell size. The reason is that the larger is the supercell size, the more free space is available for displacements.

The strong lattice relaxation significantly changed the electronic structure of the supercells. Three defect states have been found. A state is characterized as a defect state primarily because the k-projection of its wavefunction has a nearly uniform distribution over the k points in the Brillouin zone, while other bulk-

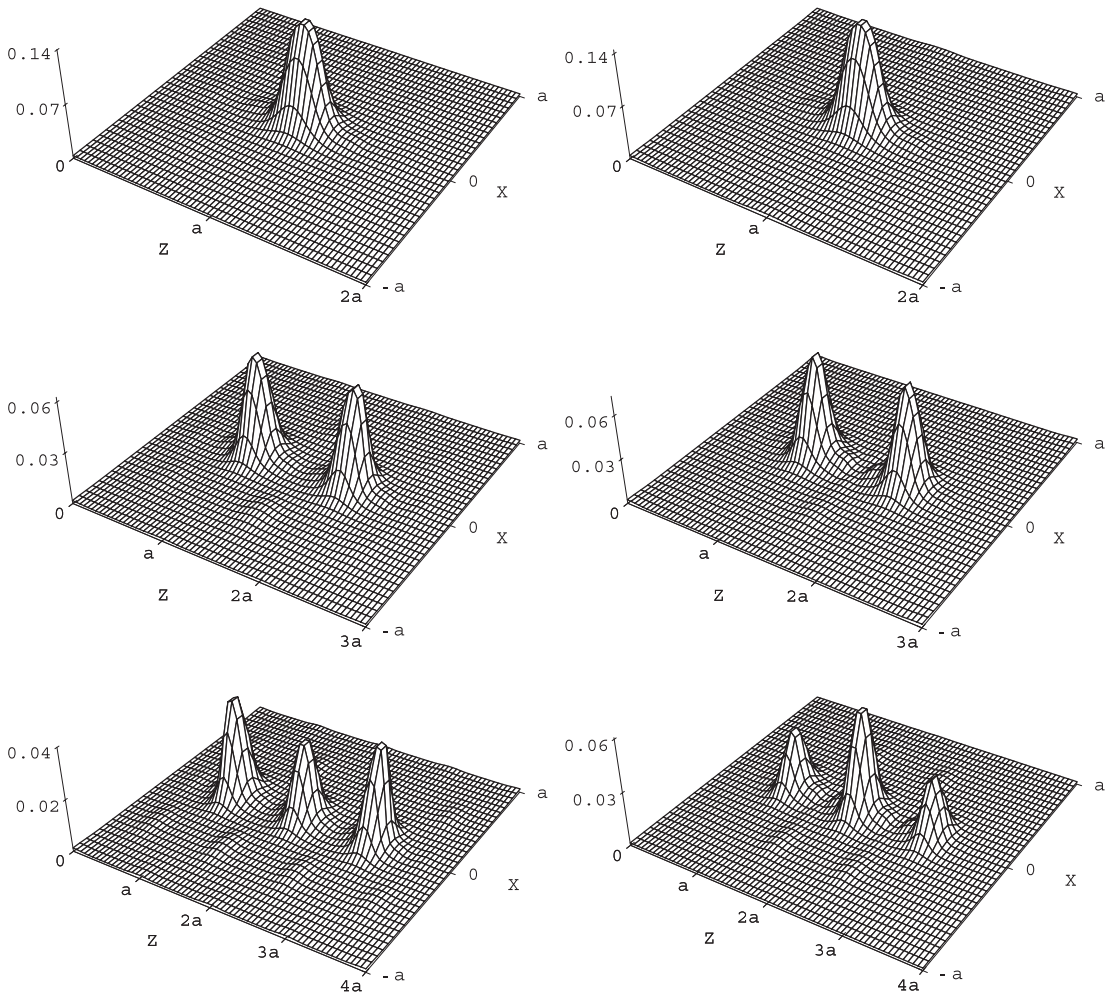

Fig. 4. Charge distribution ($|\psi|^2$), in the *z-x* plane, of the hyper-deep state E_1 for 31-atom supercell (upper row), 47-atom supercell (middle row), and 63-atom supercell (bottom row), before (left column) and after (right column) the high-lying singlet state is occupied (i.e., in the V_O^{++} and V_O^0 state). Note that the vacancy is at the origin (0,0,0).

like states tend to have the projection only at a few specific symmetrically related k points.

One of the intriguing results is the finding of a hyper-deep defect state near the a_{1g} band, since a_{1g} band is $\sim 15-17$ eV below the top of the VB. Fig. 4 shows the charge distribution (the square of the wavefunction) of this defect state. The wavefunction of this defect state (to be called E_1 hereafter) is found to be localized not on the vacancy site but on the nearby O sites along the [001] direction along which the removed O used to bond with two W atoms. Wavefunction has very little distribution at other atomic sites, which are not in the [001] axis, even though some of them are closer to the vacancy.

Beside this hyper-deep defect states, we have found two additional states, one singlet (E_2) and one doublet (E_3), in resonance with the conduction band (CB). The E_2 and E_3 levels are found to be located in between the t_{2g}^* and a_{1g}^* band. Fig. 5 shows the charge distributions typical for these defect levels in the two larger supercells. The wavefunction of E_2 is mostly localized at vacancy site, to be exact, between the vacancy and the nearest W's; while E_3 is mostly localized at the closest O's along the [010] and [100] direction (i.e., (0,a,0), and (a,0,0)). Note that E_3 is in fact similar in nature to what normally been discussed vacancy states near the band gap in many other materials [22–29], i.e., a normal excited state of the vacancy. However, E_2 should be viewed as an anti-bonding state of the vacancy configuration. The hyper-deep defect state is then a bonding state of the vacancy configuration. The formation of this bonding state can be understood as: The removal of the O at the origin effectively creates a repulsive potential for the electron at the core of the vacancy [25], which drives the "extra" electron of the nearest W away from the vacancy site along the lowest energy direction [001]. With the analogy to the situation of two off center potential wells, E_1 may be viewed as a bonding state and E_2 an anti-bonding state. To some extent, the appearance of the E_1 state here is similar to the case of an isoelectronic impurity, which was also found to have a hyper-deep bonding

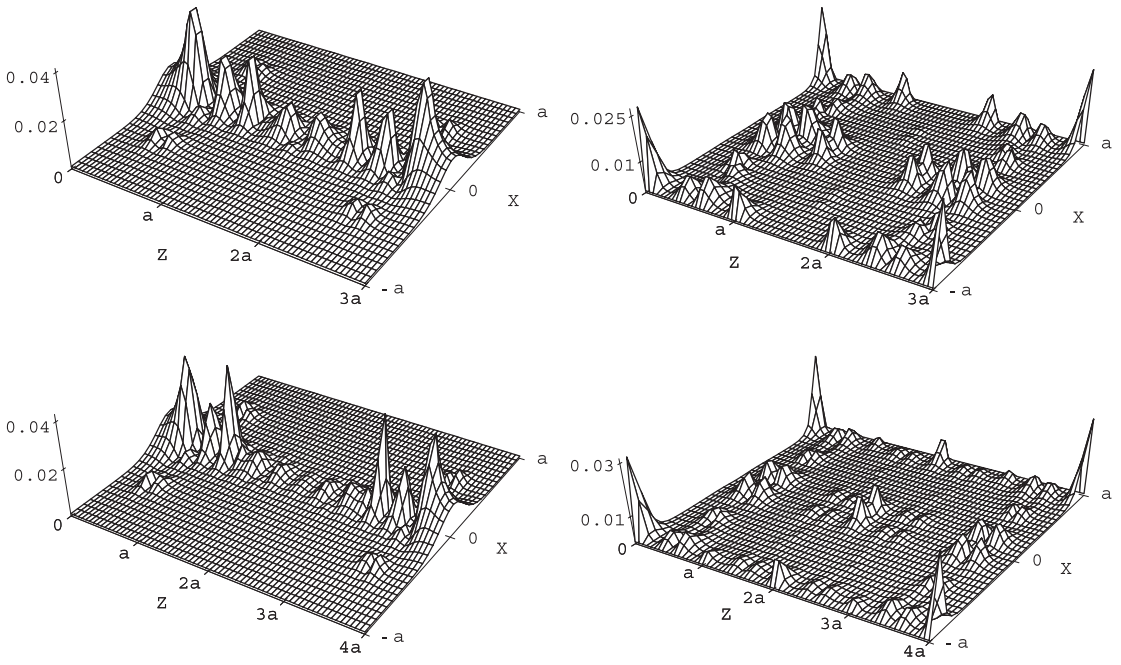

Fig. 5. Charge distribution ($|\psi|^2$), in the $z-x$ plane, of the high-lying defect state (E_2, left column) and the donor-like defect state (E_3, right column) for the 47-atom supercell (upper row) and 63-atom supercell (bottom row), with the vacancy at the V_O^o state. Note that the vacancy is at the origin (0,0,0).

and a high-lying anti-bonding localized state [30]. The band-projection analysis indicates that E_1 is primarily constructed from the states of the a_{1g} band, E_2 has the largest contribution from the high-lying a^*_{1g} anti-bonding band, but with a significant amount from the a_{1g} bonding band. Thus, this analysis further corroborates the bonding–anti-bonding relation of the E_1 and E_2 state.

According to the conventional description of a vacancy, when the E_2 state or the V_O site is unoccupied, V_O is in a charge state of V_O^{++} (positive bivalent); when occupied, in a charge state of V_O^o (neutral). These notations are conventionally adopted for describing the change in the number of electrons at the V_O site with respect to the ideal crystal. However, at the V_O site, there is actually no charge distribution for the V_O^{++} state but there is for the V_O^o state, when inspecting the total charge distribution of the system.

The second intriguing finding comes from how to allocate the two "extra" electrons. One natural option is to allow them to occupy the lowest available excited state, i.e., the bottom of the LDA CB; another one is to have them occupy the high-lying defect state, say, the E_2 state. We find between these two options not only a large swing of the nearest W atoms from one side of the ideal position to the other, as shown in Fig. 3, but also huge changes in the energies of the defect states (as large as 1–2 eV), as shown in Fig. 6. The effects on the defect state wavefunctions can also be seen in Fig. 4 for the E_1 state.

The analysis of Fig. 6 shows that for V_O^{++} the E_1 level is lower than the a_{1g} band by ~ 0.5 eV. For V_O^o, we find that the E_1 level moves from below the a_{1g} band to above. The reason can be related to inward displacement of the nearest W ions due to the attraction of the two added electrons at the "V_O site"; and those nearest O ions move back slightly, due to the restored repulsion. In the mean time, the charge distribution of E_1 at the nearby O sites along the [001] chain enhances for the 32- and 48-sites supercell and is pushed further away to the next O site along the chain for the 64-sites supercell (see the right column of Fig. 4).

As the charge state of V_O changes from V_O^{++} to V_O^o, the energy of the E_2 state itself also alter significantly (see Fig. 6). The separation between E_1 and E_2 reduces significantly, because of the drop of the electrostatic energy at the vacancy site and the raise of the electrostatic energy at those O sites along the

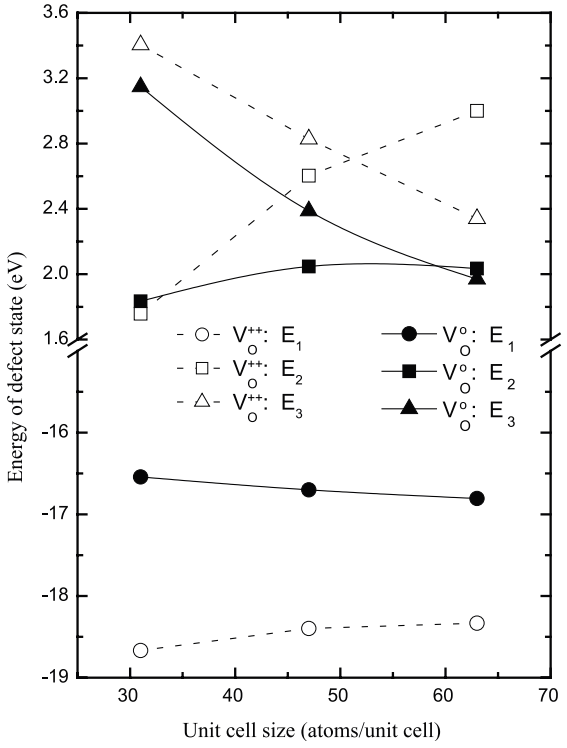

Fig. 6. The dependences of the energy levels on the supercell size and the vacancy charge state for three defects states. The energy reference is at the top of the valence band (R-point).

[001] chain. Associated with the change, the other defect state E_3 also experiences major changes both in its energy (see Fig. 6). Also, energy levels of the defects can be altered not only with the change in the charge state of the vacancy, but also the change of the supercell size, which is related to that of the displacements shown in Fig. 3.

Next, we attempt to correlate our results to those controversial issues in WO_3. Since the E_2 state is largely composed of states of the high-lying a^*_{1g} anti-bonding band, the LDA error in band gap is not expected to change the fact that it is a deep resonant state in the CB. However, the band-projection analysis for the E_3 state reveals that this state is mainly derived from the two highest VBs ($t_{1g}+t_{2u}$ and t_{2g}). Thus, if the CB moves up after the LDA error being corrected, this state should drop into the band gap and behaves as a donor state. If this situation does occur, because of its double degeneracy, in the ground state of the defect structure E_3 will be half filled, according to the

state counting described earlier. On one hand, this state is less localized in the real space, compared to E_1 and E_2; and on the other hand, it has a finite dispersion in k space even for the largest supercell. With these properties, the existence of this defect state offers a possible explanation for the observed dependence of the conductivity on the O deficiency [7]. Also, the optical transition from this bound state to conduction band states above the CB edge or the E_2 state is naturally a plausible candidate for the experimentally observed mid-gap absorption [7]. Note that the 31, 47 and 63 atom supercells correspond to the oxygen deficient WO_m with different values of the index $m = 2.875$, 2.917 and 2.9375, respectively. So, one can relate the change of energy levels of the defects with the supercell size in Fig. 6 to that of the oxygen deficiency. This can serve as possible explanation for the experimentally observed shift to lower energies of the peak value of the absorption coefficient of WO_m with decreasing the oxygen deficiency [7]. However, a quantitative comparison with experimental data is hindered by both the LDA error and the use of ordered structure.

In summary, we have found that the oxygen vacancy in WO_3 can generate three types of defect states: a hyper-deep one associated with the bonding band of the oxygen 2s states, a high-lying one associated with the anti-bonding band of oxygen 2s states, and a donor-like state associated with the valence bands near the fundamental band gap. Such a finding is expected to be general for other related oxides. The relevancy of the results is discussed with respect to the dependence of the coloration efficiency, mid-gap optical transition, and the conductivity on the oxygen vacancy in WO_3.

Acknowledgements

We thank Dr. S.H. Wei and S.H. Lee for useful discussions. The work at NREL was supported by the U.S. Department of Energy under contract No. DE-AC36-99GO10337 and at LBNL under Contract number DE-AC03-76SF00098. The computational resources were provided by the National Energy Research Scientific Computer Center.

References

[1] S.K. Deb, Appl. Opt., Suppl. 3 (1969) 192; S.K. Deb, Philos. Mag. 27 (1973) 801.
[2] C.G. Granqvist, Handbook of Inorganic Electrochromic Materials, Elsevier, Amsterdam, 1995.
[3] C.N.R. Rao, B. Raveau, Transition Metal Oxides, Structure, Properties, and Synthesis of Ceramic Oxides, 2nd ed., Wiley-VCH, New York, 1998.
[4] B.W. Faughnan, R.S. Crandall, P.M. Heyman, RCA Rev. 36 (1975) 177.
[5] O.F. Schirmer, J. Phys., Paris, Colloq. 6 (1980) 479.
[6] S.-H. Lee, H.M. Cheong, J.-G. Zhang, A. Mascarenhas, D. Benson, S.K. Deb, Appl. Phys. Lett. 74 (1999) 242.
[7] E.K.H. Salje, Eur. J. Solid State Inorg. Chem. 31 (1994) 805.
[8] L. Kopp, B.N. Harmon, S.H. Liu, Solid State Commun. 22 (1977) 677.
[9] D.W. Bullet, J. Phys. C. Solid State Phys. 16 (1983) 2197.
[10] C.-G. Zhan, F. Zheng, Theochemistry 285 (1993) 89.
[11] A. Stashans, S. Lunell, Int. J. Quant. Chemistry 63 (1997) 729.
[12] N.E. Christensen, R.A. Mackintosh, Phys. Rev., B 35 (1987) 8246.
[13] A. Hjelm, C.G. Grandqvist, J.M. Wills, Phys. Rev., B 54 (1996) 2436.
[14] F. Cora, A. Patel, N.M. Harrison, R. Dovesi, C.R.A. Catlow, J. Am. Chem. Soc. 118 (1996) 12174.
[15] F. Detraux, Ph. Ghosez, X. Gonze, Phys. Rev., B 56 (1997) 983.
[16] G.A. de Wijs, P.K. de Boer, R.A. de Groot, G. Kresse, Phys. Rev., B 59 (1999) 2684.
[17] G.A. de Wijs, R.A. de Groot, Phys. Rev., B 60 (1999) 16463.
[18] E.A. Kotomin, R.I. Eglitis, A.I. Popov, J. Phys., Condens. Matter 9 (1997) L315.
[19] R.I. Eglitis, N.E. Christensen, E.A. Kotomin, A. Postnikov, G. Borstel, Phys. Rev., B 56 (1997) 8599.
[20] Cs. Balazsi, M. Farkas-Jahnke, F. Kotsis, L. Petras, J. Pfeifer, Solid State Ionics 141 (2001) 411.
[21] F.P. Koffiberg, K. Dwight, A. Wold, Solid State Commun. 30 (1979) 433.
[22] C.A. Coulson, F.R.S., M.J. Kearsley, Proc. R. Soc., A 241 (1957) 433.
[23] N.J. Parada, G.W. Pratt Jr., Phys. Rev. Lett. 20 (1969) 180; N.J. Parada, Phys. Rev., B 3 (1971) 2042.
[24] M. Jaros, J. Phys. C 8 (1975) L550.
[25] J. Bernholc, S.T. Pantelides, Phys. Rev., B 18 (1978) 1780.
[26] S. Das Sarma, A. Madhukar, Phys. Rev. B 24 (1981) 2051.
[27] R.P. Messmer, G.D. Watkins, Phys. Rev., B 7 (1973) 2568.
[28] S.G. Louie, M. Schlüter, J.R. Chelikowsky, M.L. Cohen, Phys. Rev., B 13 (1976) 1654.
[29] G.A. Baraff, E.O. Kane, M. Schlüter, Phys. Rev. Lett. 43 (1979) 956.
[30] H.P. Hjalmarson, P. Vogl, D.J. Wolford, J.D. Dow, Phys. Rev. Lett. 44 (1980) 810.